Vps34p differentially regulates endocytosis from the apical and basolateral domains in polarized hepatic cells

Pamela L. Tuma,[1] Lydia K. Nyasae,[1] Jonathan M. Backer,[2] and Ann L. Hubbard[1]

[1]Department of Cell Biology and Anatomy, Johns Hopkins University School of Medicine, Baltimore, MD 21205
[2]Department of Molecular Pharmacology, Albert Einstein College of Medicine, New York, NY 10461

Using a microinjection approach to study apical plasma membrane protein trafficking in hepatic cells, we found that specific inhibition of Vps34p, a class III phosphoinositide 3 (PI-3) kinase, nearly perfectly recapitulated the defects we reported for wortmannin-treated cells (Tuma, P.L., C.M. Finnegan, J.-H Yi, and A.L. Hubbard. 1999. *J. Cell Biol.* 145:1089–1102). Both wortmannin and injection of inhibitory Vps34p antibodies led to the accumulation of resident apical proteins in enlarged prelysosomes, whereas transcytosing apical proteins and recycling basolateral receptors transiently accumulated in basolateral early endosomes. To understand how the Vps34p catalytic product, PI(3)P, was differentially regulating endocytosis from the two domains, we examined the

PI(3)P binding protein early endosomal antigen 1 (EEA1). We determined that EEA1 distributed to two biochemically distinct endosomal populations: basolateral early endosomes and subapical endosomes. Both contained rab5, although the latter also contained late endosomal markers but was distinct from the transcytotic intermediate, the subapical compartment. When PI(3)P was depleted, EEA1 dissociated from basolateral endosomes, whereas it remained on subapical endosomes. From these results, we conclude that PI(3)P, via EEA1, regulates early steps in endocytosis from the basolateral surface in polarized WIF-B cells. However, PI(3)P must use different machinery in its regulation of the apical endocytic pathway, since later steps are affected by Vps34p inhibition.

Introduction

Epithelial cells line all organs of the body and provide a selective barrier between the external and internal worlds. Intercellular junctions establish this barrier by cementing the cells together, thus restricting distinct cellular activities to either the apical or basolateral plasma membrane (PM)* domain. Such functional asymmetry (or polarity) reflects the differential distribution of PM proteins in the two domains. Studies identifying the molecular sorting mecha-

nisms and pathways by which newly synthesized PM proteins achieve their specific, yet asymmetric, distributions indicate that there is great plasticity among cell types and membrane protein classes (Keller and Simons, 1997; Tuma and Hubbard, 2001).

Although much less is known about how proteins are retained at their specific domains or what regulates their turnover, there seems to be plasticity in these processes also. In particular, differences in the mechanisms regulating internalization from the two domains have been described (Gottlieb et al., 1993; Jackman et al., 1994; Holm et al., 1995; Llorente et al., 1996; Shurety et al., 1996). We have been examining one such difference in polarized hepatocytes. Using the phosphoinositide 3 (PI-3) kinase inhibitors, wortmannin and LY294002, we found that endocytic trafficking of resident membrane proteins from the hepatic apical domain was under the control of PI-3 kinase activity, whereas internalization of basolateral residents was not (Tuma et al., 1999).

Of the three classes of mammalian PI-3 kinases, only classes I and III are inhibited by the relatively low wortmannin concentrations used in our published studies. Class I in-
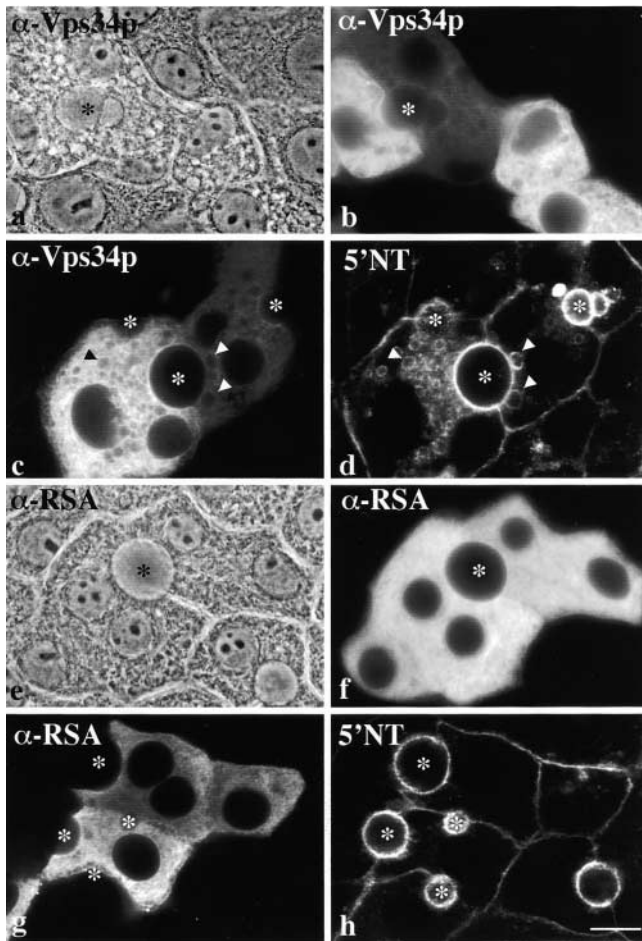
Figure 1. **Injection of anti-Vps34p induces formation of vacuoles that contain apical PM proteins.** WIF-B cells were injected with anti-Vps34p (a–d) or anti-RSA (e and f). 4 h postinjection, cells were labeled for the injected antibodies (b, c, f, and g) or 5′NT (d and h). Phase micrographs are shown in panels a and e. Arrowheads point to vacuoles containing 5′NT (d and h). Asterisks mark bile canaliculi (BCs) of injected cells. The data are representative of four experiments. Bar, 10 μm.

Figure 2. **Lysosomal membrane proteins accumulate in anti-Vps34p–induced vacuoles.** WIF-B cells were injected with anti-Vps34p (a and b) or anti-RSA (c and d). 4 h postinjection, cells were double-labeled for the injected antibodies (a and c) and endolyn-78 (b and d). Arrowheads point to vacuoles containing endolyn-78. Asterisks mark BCs of injected cells. The data are representative of three experiments. Bar, 10 μm.

cludes the p85/p110 heterodimeric kinases which consist of a 110-kD catalytic subunit associated with a regulatory 85-kD subunit. The other member is PI3K-γ, whose catalytic activity is regulated by the βγ subunits of heterotrimeric G-proteins (Fruman et al., 1998; Backer, 2000). Class III is the homologue of the sole PI-3 kinase expressed in yeast, Vps34p (Herman and Emr, 1990; Volinia et al., 1995). This kinase is also under the control of a regulatory subunit, p150 (in mammalian cells) or Vps15p (in yeast) (Herman et al., 1991; Panaretou et al., 1997).

Both the p85/p110 and Vps34p/p150 PI-3 kinases have been implicated in regulating endocytic membrane transport (Shepherd et al., 1996; Backer, 2000), preventing the direct identification of the enzyme inhibited in our wortmannin studies. To discriminate which kinase was involved, we took a direct approach and injected specific inhibitory reagents. For the class I kinases, we injected inhibitory antibodies raised against the p110α or β catalytic subunits or we injected glutathione S-transferase (GST) fusion proteins encoding the NH2-terminal SH2 (nSH2) do-
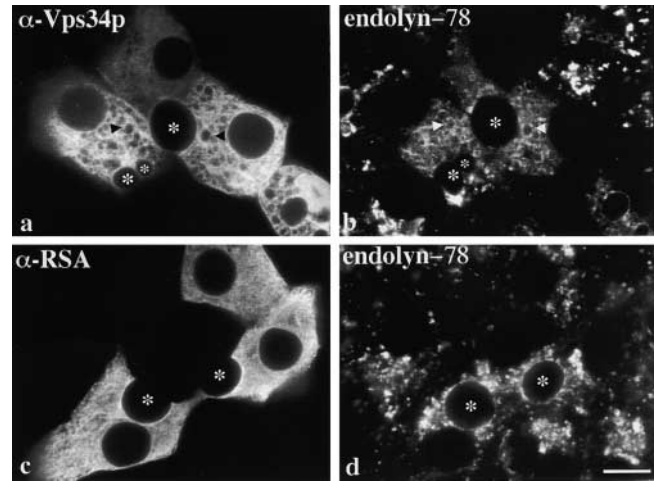
main of the p85 regulatory subunit that has been used extensively as an inhibitor of activated p110 catalytic subunits (Jhun et al., 1994; Hill et al., 2000). For the class III lipid kinase activity, we injected inhibitory Vps34p antibodies (Siddhanta et al., 1998). In vitro, these antibodies significantly and selectively decreased the catalytic activity of their respective kinases; when injected into either CHO or HepG2 cells, the antibodies inhibited different membrane transport steps (Siddhanta et al., 1998). Using these inhibitory reagents in polarized hepatic cells, we found that specific inhibition of the class III PI-3 kinase, Vps34p, led to the formation of prelysosomal vacuoles containing endocytosed resident apical PM proteins and to the transient accumulation of transcytosing apical membrane proteins in basolateral early endosomes. These results indicate that the lipid product of Vps34p, PI(3)P, regulates the two endocytic pathways differentially at an early endosomal stage from the basolateral surface, and from prelysosomes to lysosomes from the apical surface.

Results

Injection of Vps34p antibodies induces formation of vacuoles that contain apical PM and lysosomal membrane proteins

To determine which PI-3 kinase(s) was responsible for the wortmannin-induced changes we have described previously (Tuma et al., 1999), we examined the distributions of resident apical proteins and lysosomal membrane proteins in cells injected with specific inhibitory reagents. As shown in Fig. 1 a, cells injected with anti-Vps34p were heavily vacuolated 4 h after injection and these vacuoles, which were also readily apparent in cells stained for the injected antibodies (Fig. 1, b and c), strongly resembled those induced by wortmannin (Tuma et al., 1999). In the injected cells, low but detectable amounts of apical PM proteins were ob-
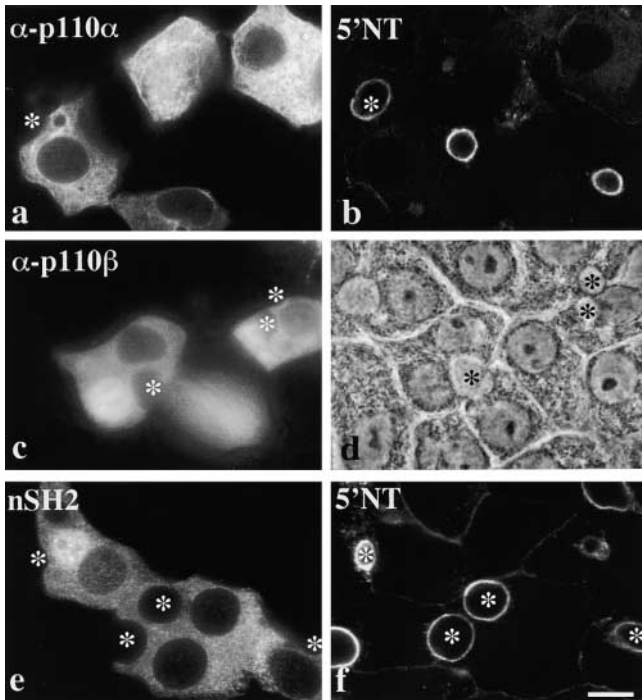
Figure 3. **WIF-B morphology and apical PM protein distributions do not change in cells injected with anti-p110α, anti-p110β, or nSH2 domains.** WIF-B cells were injected with anti-p110α (a and b) or anti-p110β (c and d) or nSH2 domains (e and f). 4 h postinjection, cells were labeled for the injected antibodies (a and c), the fusion protein (e), or 5′NT (b and f). The phase micrograph for the anti-p110β–injected cells is shown (d). Asterisks mark BCs of injected cells. The data are representative of at least three experiments. Bar, 10 μm.

Figure 4. **Anti-Vps34p and anti-p110α impair basolateral to apical transcytosis of apical proteins, but transcytosing molecules do not accumulate in vacuoles.** (A) Cells were injected with anti-Vps34p (a and b), -p110α (c and d), or -p110β (e and f) and recovered for 2 h. 5′NT molecules present at the basolateral PM were labeled with antibodies for 15 min at 4°C and the antibody–antigen complexes were chased for 3 h at 37°C. The cells were then fixed and permeabilized and the trafficked molecules visualized with secondary antibodies. Injected antibody staining is shown in a, c, and e while staining of the trafficked 5′NT is shown in b, d, and f. Asterisks indicate the BCs of injected cells. Arrowheads in panel b point to the intracellular accumulations of trafficked 5′NT in anti-Vps34p–injected cells, and the arrows in panels c and d point to unlabeled apical PM in anti-p110α–injected cells. (B) Cells were injected and labeled for 5′NT as described in the legend to A, except the antibody–antigen complexes were chased for 0, 90, or 180 min. For each time point, injected cells were scored for the relative intensity of anti-5′NT immunofluorescence (BC Staining) present at the apical PM. Black bars represent the percentages obtained from control, uninjected neighboring cells (con), while the open bars represent injected cells (inj). Only polarized cells were included in the analysis. Approximately 85–180 cells were examined for each time point. Values are expressed as the mean ± SD. Measurements were performed on at least three experiments. Bar, 10 μm.

served in vacuoles (5′NT, Fig. 1 d; and dipeptidyl peptidase IV (DPP IV), unpublished data). No changes in resident basolateral PM protein distributions were observed (unpublished data). To control for the injection process itself, cells were injected with anti–rat serum albumin (RSA). By phase (Fig. 1 e) and immunofluorescence microscopy (Fig. 1, f and g), no vacuoles formed and 5′NT distribution was normal (Fig. 1 h). Lysosomal membrane proteins also redistributed to the vacuoles induced by anti-Vps34p injection (endolyn-78, Fig. 2 b; lysosomal glycoprotein of 120 kD (LGP-120), unpublished data), but were not changed after anti-RSA injection (Fig. 2 d).

We saw no vacuole formation in cells injected with anti-p110α (Fig. 3 a) or anti-p110β (Fig. 3, c and d). Furthermore, neither 5′NT (Fig. 3 b) nor endolyn-78 distributions (unpublished data) were altered in the injected cells. To confirm that class I kinases were not regulating apical membrane dynamics, we injected another specific inhibitor, the nSH2 domain of the p85 regulatory subunit. Importantly, this domain inhibits kinase activity by a different mechanism than the antibodies and has been used extensively as an inhibitor of activated p85/p110 heterodimers (Jhun et al., 1994). Injection of the nSH2 domain had no observable effects on the morphology of injected cells (Fig. 3 e) or the distributions of 5′NT (Fig. 3 f) or endolyn-78 (unpublished data). Together, these results indicate that Vps34 specifically regulates the dynamics of resident apical PM proteins.
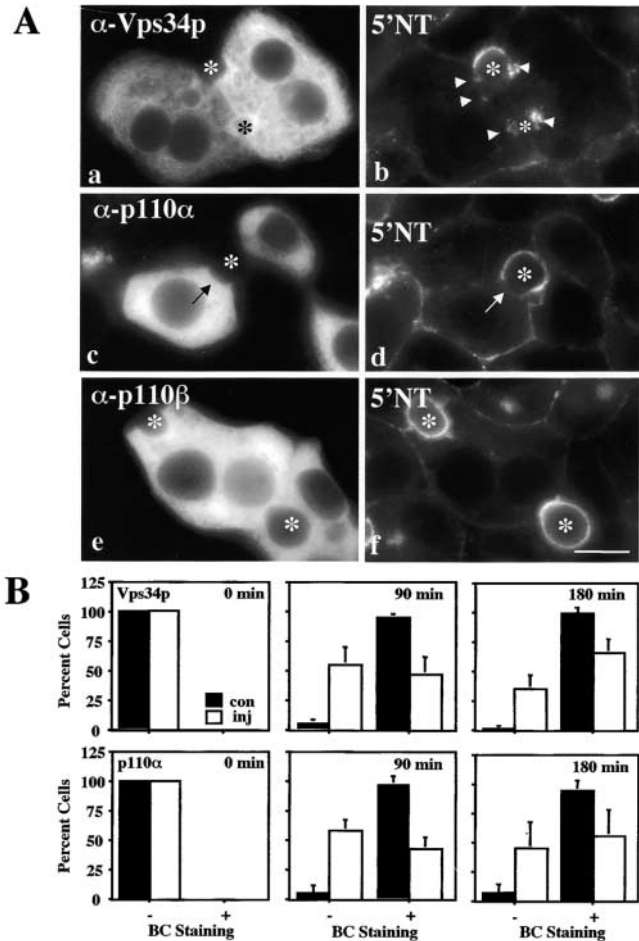
The apical PM proteins in vacuoles come from the apical PM

In our previous study with wortmannin, we found that the apical PM proteins in vacuoles came from the apical surface itself (Tuma et al., 1999). To determine whether this was also the case in anti-Vps34p–injected cells, we monitored

the fates of staged apical proteins labeled with specific antibodies. First, we sought to exclude the transcytotic pathway as the source. For these experiments, cells were injected with the inhibitory antibodies or nSH2 and allowed to recover for 2 h at 37°C (during which time vacuoles formed in anti-Vps34p–injected cells). The basolateral pool of 5′NT (those molecules en route to the apical domain) was labeled with antibodies at 4°C in live cells, the cells were warmed to 37°C and the antibody–antigen complexes chased for 3 h. The cells were fixed and permeabilized and the trafficked complexes was visualized with secondary antibodies.

Cells injected with anti-Vps34p showed altered basolateral-to-apical transcytosis, but this pathway did not contribute to the vacuolar pool of apical proteins. Trafficked 5′NT was found near the apical PM in multiple puncta that were not present in neighboring, uninjected cells (Fig. 4 b). Although >50% (51.7 ± 13.4%) of the injected cells contained the trafficked intermediates, it is important to emphasize that these structures were distinct from the large vacuoles containing apical proteins at steady state (Fig. 1 d). Furthermore, like wortmannin, anti-Vps34p was slowing but not inhibiting transcytosis (Cardone and Mostov, 1995; Hansen et al., 1995; Tuma et al., 1999). In uninjected neighbors, the apical PM stained brightly for 5′NT, but this staining was absent in injected cells (Fig. 4 b). The lag in delivery was more apparent when apical labeling was quantified (Fig. 4 B). By 90 min, ∼95% of control apical surfaces were positive for 5′NT staining, whereas in injected cells, ∼45% were labeled. After 180 min, more apical domains were labeled (∼65%) in the injected cells indicating increased delivery of 5′NT.

In cells injected with anti-p110α, p110β (Fig. 4, d and f, respectively) or nSH2 domains (unpublished data), transcytosing proteins behaved differently. Surprisingly, injection of anti-p110α impaired 5′NT transcytosis to a similar extent to that seen with anti-Vps34p (Fig. 4 B). Little to no 5′NT staining was observed at the apical surface, with a corresponding increase in staining at the basolateral surface. Furthermore, no intracellular intermediates were observed; <5% (4.5 ± 5.2%) of the anti-p110α–injected cells contained intracellular populations of trafficked 5′NT (Fig. 4 d). In anti-p110β–injected cells, apical labeling by trafficked 5′NT was morphologically (Fig. 4 f) and quantifiably (unpublished data) indistinguishable from the uninjected neighbors. Similarly, no impairment in transcytosis was observed in cells injected with nSH2 (unpublished data).

To directly determine that the apical PM was the source of the apical proteins found in anti-Vps34p–induced vacuoles, we monitored the fate of 5′NT molecules staged at the apical surface. The basolateral pool of 5′NT was labeled as described above but was followed by a prolonged 5 h chase at 37°C to allow complete apical delivery of the antibody–antigen complexes. The cells were then injected with anti-Vps34p and incubated an additional 4 h before fixation, permeabilization, and labeling with secondary antibodies to detect the trafficked complexes. As shown in Fig. 5, a and b, virtually all of the trafficked 5′NT was detected at the apical PM in control cells. Since transcytosing molecules did not accumulate in anti-Vps34p–induced vacuoles (Fig. 4), the small amount of 5′NT remaining at the basolateral surface
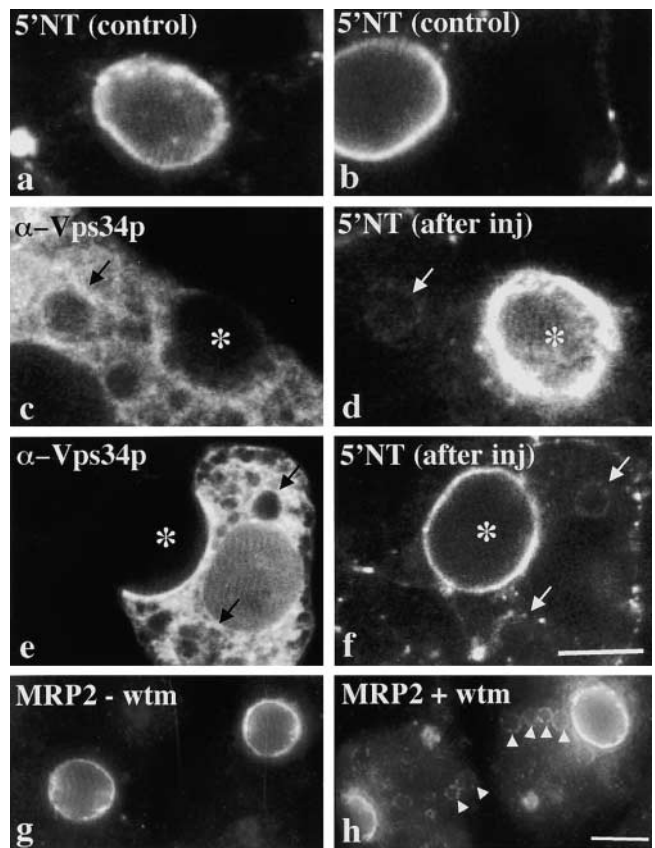

Figure 5. **The apical proteins in vacuoles come from the apical PM.** (a–f) 5′NT antibody–antigen complexes were chased to the apical PM for 5 h at 37°C. The cells shown in panels c–f were injected with anti-Vps34p and incubated an additional 4 h. In a and b, 5′NT staining in uninjected cells is shown. Cells double-labeled for the injected antibody and trafficked 5′NT are shown in c and e and d and f, respectively. Arrows are pointing to anti-Vps34p–induced vacuoles that contain apical PM proteins after the additional chase. The data are representative of four experiments. (g and h) WIF-B cells were incubated for 3 h in the absence (g) or presence of 100 nM wortmannin (wtm; h) and stained for MRP2. In untreated cells, MRP2 is detected only at the apical PM (g). Arrowheads point to MRP2-positive vacuoles in treated cells (h). Bars, 10 μm.

did not contribute to vacuolar staining. In cells injected with anti-Vps34p, vacuoles were observed (Fig. 5, c and e, arrows) that contained 5′NT (Fig. 5, d and f). Similar results were seen for trafficked aminopeptidase N (APN) (unpublished data). Thus, the apical PM proteins found in vacuoles came from the apical PM. The relatively low level of 5′NT vacuolar accumulation likely reflects its low degradative rate ($t_{1/2}$ = ∼2 d; unpublished data) and slow transport to lysosomes.

To further confirm these results, we examined the distributions of the polytopic apical PM protein, multidrug resistance–associated protein 2 (MRP2), in wortmannin-treated WIF-B cells. Importantly, this apical protein is localized exclusively to the apical PM in untreated WIF-B cells (Fig. 5 g). After treatment for 3 h, MRP2 staining was observed on large wortmannin-induced vacuoles (Fig. 5 h), indicating that the source of apical proteins in vacuoles was the apical PM. These data show that specific inhibition of Vps34p nearly perfectly recapitulated the defects we reported for
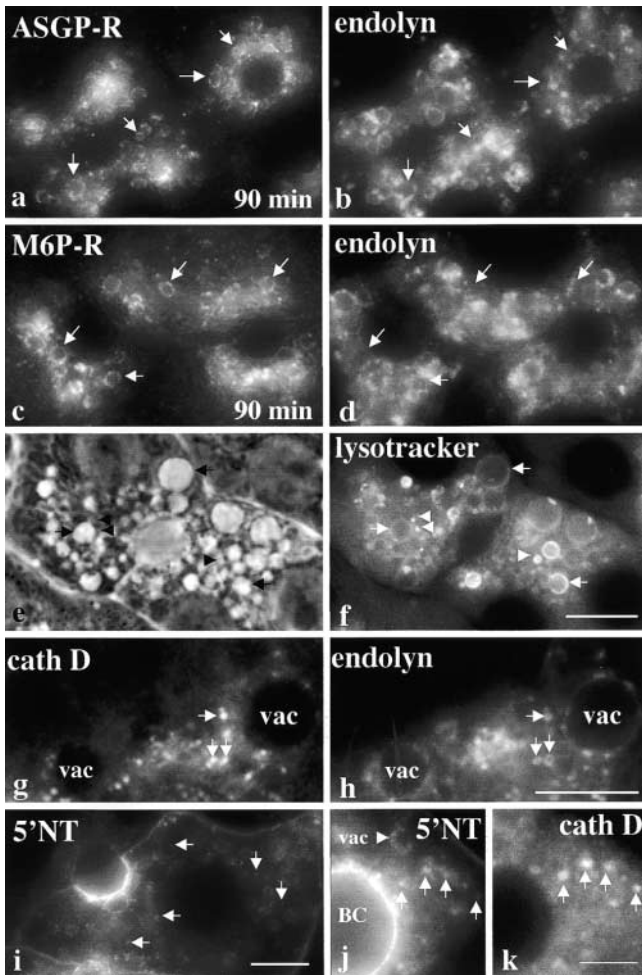
Figure 6. **Wortmannin induces formation of distinct vacuole populations, but does not alter mature lysosome morphology.** In panels a–d, cells were treated for 90 min with 100 nM wortmannin. The relative distributions of endolyn-78 to ASGP-R (a and b) or M6P-R (c and d) are shown. Arrows in a and b are pointing to structures that only contain ASGP-R, and in c and d that contain only M6P-R. In e–k, cells were treated for 180 min with 100 nM wortmannin. In e and f, 50 nM lysotracker was added in the final 30 min of wortmannin treatment. Lysotracker staining of acidic compartments in live cells is shown in panel f, and the corresponding phase image in panel e. Enlarged images of wortmannin-treated cells double-labeled for endolyn-78 (h) and cathepsin D (cath D, g) are shown. Arrowheads indicate small puncta containing endolyn at the surface and cathepsin D in the lumen. In panels i–k, 50 μM leupeptin was included hourly in the wortmannin incubations to inhibit acid hydrolase activity. Arrows are pointing to small puncta that contain 5'NT in panel i. Arrows in the enlarged, double-labeled images in j and k are pointing to the small 5'NT-positive puncta that also contain cathepsin D. The data are representative of at least three experiments. Bars, (a–f and i) 10 μm; (g and h) 2 μm; and (j and k) 5 μm.

wortmannin-treated cells and indicate that Vps34p regulates two stages of apical membrane dynamics: apical endocytic trafficking and basolateral to apical transcytosis.

Vps34p differentially regulates endocytosis from the apical and basolateral surfaces

To better define the steps in endocytosis that PI(3)P lipids were regulating in polarized WIF-B cells, we established the intermediates that wortmannin (and anti-Vps34p) treatment
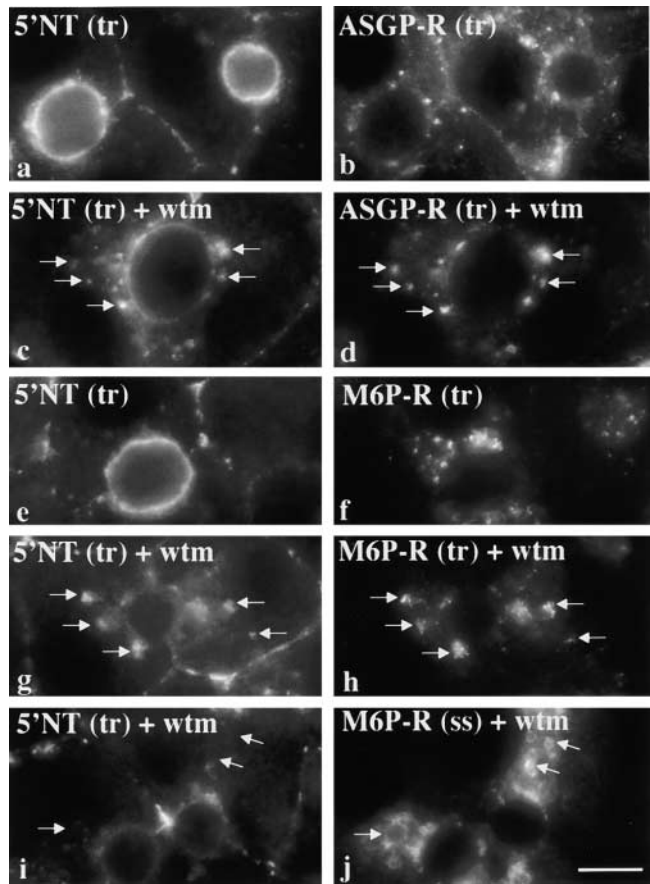

Figure 7. **Transcytosing apical proteins and recycling receptors internalized from the basolateral PM accumulate in basolateral early endosomes in wortmannin-treated cells.** WIF-B cells were treated in the absence (a, b, e, and f) or presence (c, d, and g–j) of 100 nM wortmannin for 2 h. 5'NT and ASGP-R (a–c) or 5'NT and M6P-R (e–h) at the basolateral PM were colabeled for 1 h at 37°C in the continued absence or presence of wortmannin. Arrows are pointing to structures containing both trafficked 5'NT and ASGP-R (c and d) or both 5'NT and M6P-R (g and h). In i and j, 5'NT present at the basolateral PM was continuously labeled for 1 h at 37°C in the presence of wortmannin and its distributions were examined relative to M6P-R at steady state. The data are representative of at least three experiments. Bar, 10 μm.

induced. In our earlier study, we reported that wortmannin treatment for 180 min mainly led to formation of vacuoles containing lysosomal and apical PM proteins. However, we observed transient early or late endosomal vacuole populations after shorter incubations. Neither population overlapped extensively with the vacuoles marked by endolyn-78. After 90 min of wortmannin treatment, asialoglycoprotein receptor (ASGP-R) (Fig. 6, a and b) and mannose 6-phosphate receptor (M6P-R) (Fig. 6, c and d) distributed to vacuoles distinct from those containing endolyn-78.

Since previous studies have shown that vacuoles containing lysosomal membrane proteins were not mature lysosomes, but enlarged prelysosomes (Reaves et al., 1996), we examined lysosome morphology in wortmannin-treated WIF-B cells. We first visualized all acidic compartments using lysotracker and identified two compartments: large vacuoles whose rims were stained and smaller, homogeneously stained structures (Fig. 6, e and f). To determine whether the smaller structures

Figure 8. EEA1 is localized to endosomes near the apical PM and the cell periphery that are biochemically distinct. WIF-B cells were double-labeled for EEA1 and ASGP-R (a–d), EEA1 and M6P-R (e–h), EEA1 and rab5 (i–l), or EEA1 and syntaxin13 (syn 13; m–p). In a–c, e–g, i–k, and m–o, the images were focused at the BC, whereas in d, h, i, and p, they were focused at the cell periphery. The merged images from a b, e f, i, j, m, and n are shown in c, g, k, and o, respectively. Only the merged images taken at the cell periphery are shown in d, h, i, and p. In panels q–t, EEA1 steady state distributions (r) are shown relative to endolyn-78 molecules that have been trafficked to the SAC (s). The merged image is shown in panel t. The data are representative of at least three experiments. Bar, 10 μm.
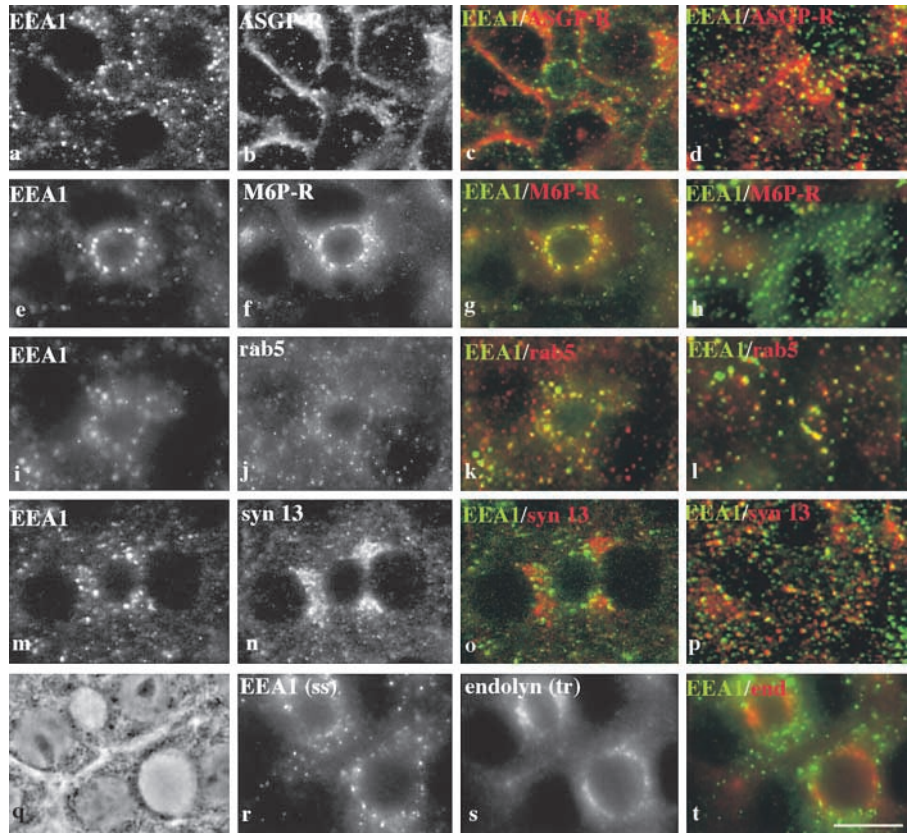
were mature lysosomes (also called dense core lysosomes; Reaves et al., 1996), we labeled treated cells for acid hydrolases. As shown in Fig. 6 g, cathepsin D distributed to small puncta that were distinct from the large, endolyn-78–positive vacuoles (Fig. 6 h). In these enlarged images, we also saw that endolyn-78 was present in the smaller, cathepsin D–positive structures. In some cases, the limiting membrane was positive for endolyn-78, whereas cathepsin D labeled only the lumen (arrows in Fig. 6, g and h). Furthermore, when 5'NT distribution was examined in treated cells in the presence of leupeptin (to inhibit lysosomal hydrolase activity), additional staining was observed in small puncta (Fig. 6 i). Double labeling with cathepsin D revealed that these structures were lysosomes, indicating that resident apical proteins were delivered to functional lysosomes (Fig. 6, j and k). Together, these results imply the presence of at least four endocytic intermediates in WIF-B cells: early endosomes (ASGP-R+), late endosomes (M6P-R+), prelysosomes/multivesicular bodies (MVBs) (endolyn-78+), and mature lysosomes (endolyn-78+, cathepsin D+; see Fig. 10). Since the apical PM proteins were detected at later time points in vacuoles that contained only endolyn-78, we conclude that they accumulated in prelysosomes before delivery to lysosomes.

In contrast to the resident apical proteins, the transcytosing apical proteins accumulated transiently in other intracellular structures. To date, only two transcytotic intermediates have been defined in polarized hepatic cells: basolateral early endosomes and the subapical compartment (SAC) (see Fig. 10; Barr et al., 1995; Ihrke et al., 1998). Since the SAC was unchanged by wortmannin treatment (Tuma et al., 1999), it was likely that the transcytosing proteins accumulated in ba-

solateral early endosomes. To test this possibility, we simultaneously monitored the trafficking of transcytosing apical proteins and ASGP-R or M6P-R from the basolateral surface. If the block occurred early in endocytic transport, these proteins, with different final destinations, should have accumulated in the same structures. Cells were pretreated for 2 h with 100 nM wortmannin. Antibodies to the different markers were then applied continuously for an additional hour at 37°C in the presence of wortmannin and their distributions were determined. As described previously (Ihrke et al., 1998) and shown in Fig. 7, 5'NT (Fig. 7, a and e), ASGP-R (Fig. 7 b), and M6P-R (Fig. 7 f) were delivered to their resident compartments in control cells (the apical PM, early and late endosomes, respectively). In treated cells, trafficked 5'NT and ASGP-R accumulated in the same intracellular compartments (Fig. 7, c and d) as did 5'NT and M6P-R (Fig. 7, g and h). Similar results were observed in cells injected with anti-Vps34p (unpublished data). Importantly, the steady state distribution of M6P-R in treated cells remained mostly distinct from the trafficked 5'NT (Fig. 7, i and j) and by extension, the trafficked M6P-R (compare Figs. 7, h and j), indicating that the dynamics of the late endosomal protein were inhibited at an earlier step. From these results, we conclude that wortmannin and anti-Vps34p impaired an early step in basolateral endocytosis in WIF-B cells (see Fig. 10).

Apical and basolateral early endosomes are biochemically distinct

Current models of the role played by PI(3)P lipids in mammalian cell endocytosis focus on early endosomal antigen 1 (EEA1), a PI(3)P-binding protein whose activity appears to

be required in early endosome fusion events (Corvera and Czech, 1998; McBride et al., 1999; Stenmark and Aasland, 1999; Backer, 2000). Although our results pointing to a block at an early stage in basolateral endocytosis are consistent with such models, those results indicating a block in late endocytic transport are not. Furthermore, there is a paradox between the results of wortmannin treatment in vitro, where EEA1 activity and membrane fusion are inhibited, and in cells, where large membrane vacuoles form. This latter phenomenon implies that membrane fusion is not inhibited in vivo.

To begin sorting out this paradox, we examined EEA1 distributions in WIF-B cells (see Fig. 10). In control cells, EEA1 was found on two membrane populations: on large puncta near the apical PM (Fig. 8, a, e, i, m, and r) and on smaller structures in the cell periphery (Fig. 8, d, h, l, and p). As shown in Fig. 8, a–c, the large, apical EEA1–positive puncta minimally colocalized with ASGP-R, another early endosome marker, whereas substantial overlap of the staining patterns was observed in the cell periphery (Fig. 8 d). Surprisingly, the staining patterns for EEA1 and M6P-R (a late endosome marker) almost completely overlapped near the apical surface (Fig. 8, e–g). In contrast, very little M6P-R was detected in the cell periphery and no colocalization with EEA1 was observed (Fig. 8 h). We also determined the relative distributions of other regulators of endocytosis, rab5 and syntaxin13, and observed rab5 staining on both EEA1-positive populations (Fig. 8, i–l). However, syntaxin13 was found with EEA1 only in the cell periphery (Fig. 8, m–p).

Due to the close proximity of the EEA1-positive structures to the apical surface, we sought a way to determine whether they were distinct from the transcytotic intermediate, the SAC. Since basolaterally internalized endolyn-78 is delivered to SAC before its transport to lysosomes (Ihrke et al., 1998), we determined the distribution of trafficked endolyn-78 relative to that of EEA1. The basolateral pool of endolyn-78 was continuously labeled with antibodies for 1 h at 37°C and then visualized with secondary antibodies. As shown in Fig. 8 s, a substantial proportion of the endoyn-78 population was present near the apical surface in structures corresponding to the SAC (Ihrke et al., 1998). However, these structures were clearly distinct from those labeled with EEA1 (Fig. 8 t). Thus, the SAC and the EEA1 apical endosomes are distinct compartments.

To further understand how PI(3)P depletion was perturbing endocytosis, we examined EEA1 distributions in WIF-B cells treated with wortmannin or anti-Vps34p antibodies. To do so biochemically, we prepared cytoplasmic and total membrane fractions from control cells or cells treated with 100 nM wortmannin and blotted them with antibodies recognizing the COOH- (Fig. 9 A) or NH$_2$-terminal domain (unpublished data) of EEA1. Greater than 75% of EEA1 was found in the soluble fraction using either antibody (lanes 1 and 2). As reported previously (Patki et al., 1997), the majority of the membrane-associated EEA1 population was eluted after incubations with wortmannin (lanes 3–8), however, ~8% of the pelleted population (~2% of the total) remained associated (compare lane 2 with 4, 6, and 8). The morphological distributions of EEA1 also changed in treated cells. Although the overall signal decreased, a signifi-
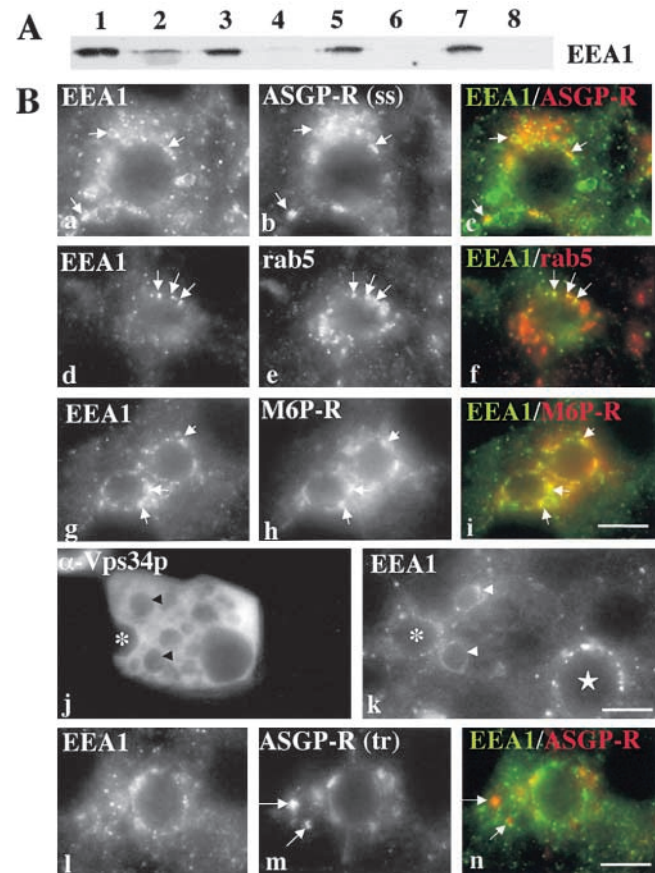

Figure 9. **Wortmannin and injection of anti-Vps34p alter EEA1 distributions.** (A) Cytosolic (lanes 1, 3, 5, and 7) and membrane fractions (lanes 2, 4, 6, and 8) were prepared from WIF-B cells treated for 0 (lanes 1 and 2), 30 (lanes 3 and 4), 60 (lanes 5 and 6), or 120 min (lanes 7 and 8) with 100 nM wortmannin. Equal volumes of the supernatant and pelleted fraction were loaded and immunoblotted with anti-EEA1. (B) WIF-B cells were incubated for 90 or 180 min with 100 nM wortmannin (a–f and g–i, respectively). Cells were fixed, permeabilized, and double-labeled for EEA1 and ASGP-R (a and b), rab5 (d and e), or M6P-R (g and h). Merged images are shown in c, f, and i. Arrowheads point to structures containing both EEA1 and the indicated marker. WIF-B cells were injected with anti-Vps34p, and after 4 h were double-labeled for the injected antibodies (j) and EEA1 (k). Images were focused at slightly different focal planes to better visualize the injected cell in panel j, and EEA1 vacuolar staining in panel k. Arrowheads point to vacuoles containing EEA1. The asterisk marks the BC of the injected cell and the star marks the BC of an uninjected cell. In panels l and m, cells were treated with 100 nM wortmannin for 120 min. ASGP-R at the basolateral surface was continuously labeled with antibodies for an additional hour in the presence of wortmannin. Trafficked ASGP-R distributions (m) were determined relative to EEA1 at steady state (l). The merged image is shown in n. The data are representative of at least three experiments, except in j and k, which are representative of two experiments. Bar, 10 μm.

cant fraction remained associated with small puncta and large vacuoles located near the apical PM; little to no staining was observed in the periphery (unpublished data and see below). In wortmannin-treated cells, EEA1 staining partially colocalized with ASGP-R (Fig. 9 B, a–c), but significantly overlapped with rab5 (Fig. 9 B, d–f). The conditions used to detect rab5 were not optimal for EEA1 detection, such that EEA1 staining in panel d was less intense than in other pan-

els. Nonetheless, nearly every EEA1-positive structure detected also contained rab5. Although the M6P-R–positive compartments were less discrete and more tubulated in treated cells (Fig. 9 B, h), there was also considerable overlap between EEA1 and M6P-R staining patterns (Fig.9 B, g–i). EEA1 was also detected in vacuoles that contained apical PM proteins in wortmannin-treated (unpublished data) and anti-Vps34p–injected cells (Fig. 9 B, j and k). 4 h after injection, EEA1 staining was visible on large vacuoles, whereas in the uninjected neighbor, only small puncta were observed (Fig. 9 B, k).

If the mechanisms regulating endocytosis from the basolateral domain are consistent with current models, EEA1 in treated cells should be dissociated from early endosomes that contain the accumulated trafficked molecules (see Fig. 7). As described above, cells were pretreated for 2 h with 100 nM wortmannin and anti–ASGP-R was continuously applied for an additional hour at 37°C in the presence of wortmannin. No overlap was seen between EEA1 at steady state and trafficked ASGP-R (Fig. 9 B, l–n). However, EEA1 remained associated with the apically located, M6P-R–positive structures, suggesting it remained functional in endocytosis from the apical domain so that blocks in late endocytic transport were revealed.

Discussion

By adopting a microinjection approach, we determined that specific inhibition of the class III PI-3 kinase, Vps34p, in polarized WIF-B cells led to the formation of prelysosomal vacuoles containing endocytosed resident apical PM proteins, and also to the transient accumulation of transcytosing apical membrane proteins in basolateral early endosomes. These results indicate that the lipid product of Vps34p, PI(3)P, regulates the two endocytic pathways differentially at an early endosomal stage in the basolateral arm, and later in the apical arm. In support of this conclusion, marker analysis of the PI(3)P-binding protein, EEA1, and other known regulators of early endocytosis revealed biochemical differences between early apical and basolateral endosomes. Furthermore, EEA1 was differentially retained on apical, but not basolateral, early endosomes when PI(3)P was depleted from WIF-B cells. From these combined results, we conclude that regulation by EEA1 and PI(3)P of the basolateral endocytic pathway in polarized hepatic cells is consistent with a current model of early endosomal events, but that other mechanisms/players must be acting in the apical pathway of polarized WIF-B cells.

Vps34p differentially regulates endocytosis from the apical and basolateral domains

The current model of PI(3)P's role in endocytosis invokes recruitment of Vps34p/p150 by activated rab5 to the sites of endosome–endosome fusion and local production of PI(3)P (Corvera and Czech, 1998; Stenmark and Aasland, 1999; McBride et al., 1999; Backer, 2000). EEA1 is then recruited to these sites where PI(3)P and rab5 binding stabilize its membrane association. The stabilized EEA1 molecules then form oligomers that coordinate the formation of a large vesicle docking site also containing NSF and syntaxin13, all of

which drive endosome fusion. Thus, in nonpolarized cells, when PI(3)P lipids were depleted by wortmannin, EEA1 association with early endosomes was lost and the subsequent events were affected. Likewise, we found that EEA1 dissociated from basolateral early endosomes in treated WIF-B cells; concomitantly we observed delayed progression of three markers from the basolateral surface. All of these results are consistent with the current model.

In contrast, the block we observed at a late endocytic step in the apical pathway is not consistent with the existing model. Disruption of EEA1 function in the fusion of early endosomes arising from the apical surface should have blocked an earlier step in the pathway. However, a subpopulation of EEA1 near the apical surface remained membrane-bound under PI(3)P-depleting conditions, suggesting that the protein remained active and allowed progression of endocytosed proteins along the apical route, thereby revealing a block downstream.

These results raise the following question: what mechanism retains EEA1 on the apical endosomes? A simple explanation is that residual Vps34p activity generated sufficient PI(3)P at this location to support EEA1 binding and function. Alternatively, since EEA1 encodes two rab5 binding domains, and rab5 labeled similar apical structures in treated cells to those with residual EEA1, the presence of rab5 alone might be sufficient to retain the protein. However, we were unable to localize syntaxin13, another important player in the current model, to apical endosomes under any conditions, implying that a different t-SNARE might be serving the docking/fusion role in this pathway. Together these results point to a different mechanism operating in the apical pathway.

Although the defects observed in apical endocytic trafficking do not conform to the current model for mammalian cells, they are strikingly similar to the endocytic defects observed in yeast expressing temperature-sensitive Vps34p alleles (Wurmser and Emr, 1998). At the restrictive temperature, endocytosis of the lipophilic dye, FM4-64 was impaired and accumulated in prevacuolar compartments. Similarly, vacuole delivery of the PM a-factor transporter, Ste6p, was impaired at a late endocytic step. Ultrastructural analysis further revealed an accumulation of aberrant membrane compartments at the nonpermissive temperature. Are these structures equivalent to prelysosomes? Does Vac1p (the yeast EEA1 homologue) remain membrane-associated at the restrictive temperature?

In addition to the differential effects of Vps34p inhibition we observed in this study, marker analysis points to important biochemical differences between apical and basolateral early endosomes in WIF-B cells (Fig. 10). Not only was syntaxin 13 absent from the apically located endosomes, but these structures also contained the late endosomal marker, M6P-R. The presence of both early and late endocytic markers on the same structure is a puzzle. Perhaps the early endocytic intermediates at the apical surface are less distinct than those at the basolateral domain and/or the markers are present on different domains of the same organelle that are specialized for specific membrane transport/sorting functions. Alternatively, the presence of M6P-R on the apically-located puncta may reflect a rate-limiting step in the traf-
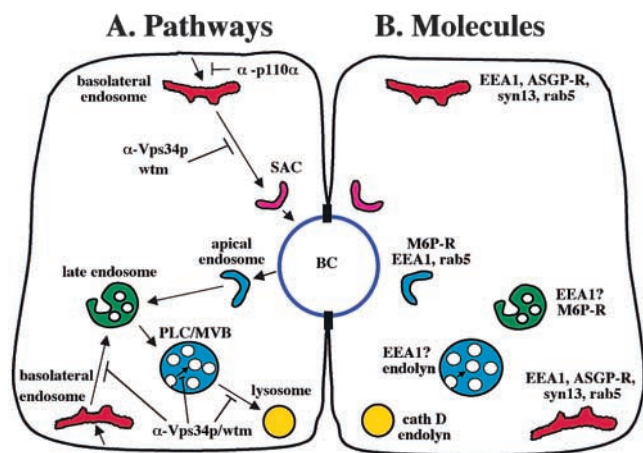
Figure 10. **Endocytic and transcytotic pathways in polarized hepatic cells.** (A) The intermediates of the transcytotic (top of cell) and endocytic intermediates (bottom of cell) are shown with arrows indicating possible transport routes. (B) The specific markers localized to these intermediates are indicated. Only two intermediates in the basolateral-to-apical transcytotic pathway have been identified: the basolateral early endosome and SAC. We propose that basolateral endocytosis proceeds sequentially through four intermediates: basolateral early endosomes, late endosomes, prelysosomes/MVB, (PLC/MVB) and finally, lysosomes. We further propose that apical endocytosis proceeds through an apical early endosome that is distinct from both the basolateral early endosome and the SAC, and converges with the basolateral endocytic pathway in M6P-R–positive late endosomes. The possible transport blocks imposed by wortmannin, anti-Vps34p, or anti-p110α are indicated in A.

ficking of this recycling receptor through the apical early endosome that it does not encounter when trafficking through basolateral early endosomes. Thus, M6P-R is not serving as a late endosomal marker in the apical endocytic pathway.

Does Vps34p differentially regulate endocytosis in other polarized epithelial cells?

Our results in hepatic cells lead to several questions. Are the apical and basolateral pathways in other polarized epithelial cells also differentially regulated by Vps34p? Wortmannin treatment of MDCK, Caco2 and FRT cells inhibited transcytosis in both directions, but the specific steps that were perturbed were not identified (Cardone and Mostov, 1995; Hansen et al., 1995). We reported that vacuoles formed in wortmannin-treated MDCK cells, but did not characterize the compartment. A related question is whether domain-specific proteins that are expressed in nonpolarized cells exhibit differential responses to Vps34p inhibition? Too few membrane proteins have been examined to currently answer this last question.

Like in WIF-B cells, EEA1 exhibits a polarized distribution in MDCK cells and is localized to basolateral and apical early endosomes that also contain rab5 (Leung et al., 2000). Importantly, the apical early endosome in MDCK cells is also biochemically distinct from the apical-recycling endosome (ARE), because neither EEA1 nor rab5 were found on the ARE. Furthermore, both apical-recycling receptors and basolateral-to-apical–transcytosing molecules pass through the ARE as the last stop before delivery to the apical PM, whereas only the transcytosing proteins were excluded from the apical early endosome. Thus, just as the apical early endosome is distinct from the ARE in MDCK cells, the WIF-B apical endosome identified in this study is distinct from the SAC. However, unlike the ARE, there is currently no evidence to support a role for the SAC in apical recycling (Barr et al., 1995). An open question is whether ARE/SAC and apical early endosomes are present as distinct compartments in nonpolarized cells.

Do the apical and basolateral endocytic pathways intersect in hepatic cells?

The intersection of the apical and basolateral degradative endocytic pathways has been well-characterized in polarized MDCK cells and absorptive intestinal cells in situ (Bomsel et al., 1989; Parton et al., 1989; Fujita et al., 1990). In particular, fluid phase markers internalized from either domain in MDCK cells found to converge in late endosomes and with increased incubation times were detected in lysosomes (Bomsel et al., 1989; Parton et al., 1989), indicating that the two pathways intersected at late endosomes and shared the subsequent endocytic intermediates en route to lysosomes. However, the extent to which the endocytic intermediates are shared by molecules internalized from either domain in hepatic cells is not known. Recently, apically internalized markers were detected in hepatocytes in situ after retrograde infusion via the bile duct (Rahner et al., 2000). Confocal analysis suggested that the apical markers were delivered to late endosomes and/or lysosomes that also received basolaterally internalized fluid phase markers. In our study, we identified at least four intermediates of the basolateral endocytic pathway in WIF-B cells (Fig. 10); these compartments are similar to those described in hepatocytes in situ (Wall and Hubbard, 1985; Dunn et al., 1986). From these combined results, we propose that markers internalized from both PM surfaces converge in late endosomes and proceed through prelysosomes to mature lysosomes (Fig. 10).

Class IA kinases and membrane traffic

Injection of p110α antibodies impaired basolateral-to-apical transcytosis of 5′NT as did anti-Vps34p injection. However, increased 5′NT basolateral surface staining was observed with no corresponding intracellular accumulations of transcytosing 5′NT. This result suggests that Vps34p and p110α act at separate steps of the pathway, with p110α possibly acting at internalization (Fig. 10). Why did injected nSH2 have no effect on transcytosis? Since this domain in p85 mediates binding of the regulatory subunit to activated receptor tyrosine kinases and their substrates which then activate p110 (Rordorf-Nikolic et al., 1995), its lack of effect is significant. Unlike the antibodies that should block all catalytic activity, the nSH2 domains were not expected to inhibit p85/p110 basal activity. The nSH2 domains were also not expected to disrupt activation of p110 kinase activity by activated CDC42 binding to p85 (Zheng et al., 1994). This is particularly important given the recent role described for CDC42 in polarized protein trafficking (Kroschewski et al., 1999). Thus, regulation of p85/p110 by non-SH2–mediated interactions may be important for transcytosis in polarized cells. Alternatively, the levels of injected nSH2 were not high enough to be inhibitory or this domain does not function as a dominant negative inhibtor in WIF-B cells.

Regulation of membrane homeostasis by PI(3)P lipids

Some puzzling issues remain. First, the inhibition by wortmannin or anti-Vps34p observed at the different transport steps is not complete. That is, transcytosing apical proteins eventually reach the apical PM and internalized resident apical proteins are eventually delivered to lysosomes for degradation. One explanation is that the class II PI-3 kinases that are insensitive to anti-Vps34p injection or low wortmannin concentrations are producing sufficient levels of PI(3)P to maintain a small flow of membrane transport. Alternatively, PI(3)P lipids are not an absolute requirement for membrane transport; they, and the proteins they recruit, merely facilitate or increase the efficiency of the process.

Another puzzle is the basis for formation of transiently and/or permanently enlarged compartments when PI(3)P levels are altered. One explanation is that vesicle transport to a compartment occurs while the corresponding efflux from the compartment is impaired. Consistent with this possibility is the finding that pretreatment with nocodazole blocks vacuole formation in wortmannin (Tuma et al., 1999) and anti-Vps34p–treated cells (unpublished data). Thus, vacuole formation predominantly results from defects in vesicle-mediated transport. Although this explanation accounts for the formation and subsequent enlargement of the endolyn-78–positive prelysosomes, it does not account for the transient nature of the early and late endosomal vacuoles. One possibility is that vacuole formation may also reflect an altered distribution of functional proton pumps in treated cells. Hepatic lysosomes and endosomes are acidified by specific sets of H(+)-ATPases (Van Dyke, 1996). The proton gradients they establish likely provide the energy necessary for transport of ions or solutes into and out of endosomes and lysosomes by specific transporters. As we showed in this study with lysotracker, and others have shown with acridine orange (Brown et al., 1995), wortmannin does not dissipate the pH gradient across the endosome or lysosome membrane. In fact, treatment with the proton-ATPase inhibitor, bafilomycin, not only prevented vacuole formation, but also rapidly collapsed preformed vacuoles (unpublished data). Thus, compartment acidification is required for vacuole formation and maintenance. Accordingly, transient vacuole formation may reflect imbalances in the net uptake of ions and solutes resulting from changes in the numbers of transporters and proton pumps present in each compartment. Such altered steady state distributions may be explained by the defects in membrane trafficking caused by PI(3)P. Alternatively, PI(3)P may be directly required for proper pump and transporter function, as has been demonstrated for sister of P-glycoprotein and MRP2 (Misra et al., 1999). In this case, depletion of PI(3)P from membranes may differentially inhibit pump or transporter activity. Whatever the explanation, it is clear that PI(3)P plays many important regulatory roles in membrane traffic in polarized hepatic cells.

Materials and methods

Materials and antibodies

10 mM wortmannin in DMSO and 5 mM leupeptin in 10% DMSO (Sigma-Aldrich) were stored at −20°C. Antibodies were from the following sources: anti-RSA from Cappel Research Products; Alexa-conjugated secondary antibodies were from Molecular Probes; monoclonal anti-EEA1 were from Transduction Laboratories. The antibodies recognizing EEA1, 5′NT, MRP2, M6P-R, rab5, syntaxin13, and cathepsin D were from S. Corvera, (University of Massachusetts, Worcester, MA), J.P. Luzio (Cambridge University, Cambridge, UK), D. Keppler (Deutsches Krebsforschungszentrum, Heidelberg, Germany), P. Nissley (National Institutes of Health, Bethesda, MD), M. Wessling-Resnick and G. Quellhorst (Harvard School of Public Health, Boston, MA), R. Scheller and V. Prekeris (Stanford University School of Medicine, Stanford, CA), and J. Blum and P. Stahl (Washington University School of Medicine, St. Louis, MO), respectively. LGP-120 polyclonal antibodies were from W. Dunn (University of Florida, Gainesville, FL) and LGP-120 monoclonal antibodies (GM10) were from K. Siddle and J. Hutton (University of Cambridge, Cambridge, UK). The SH2–GST fusion protein and antibodies against p110α, p110β, and Vps34p were prepared in the Backer laboratory and have been described elsewhere (Siddhanta et al., 1998; Hill et al., 2000). Antibodies against APN, ASGP-R, endolyn-78, DPP IV, and GST were prepared in the Hubbard laboratory and have been described elsewhere (Barr and Hubbard, 1993; Ihrke et al., 1993, 1998; Fujita et al., 1998).

Cell culture

WIF-B cells were grown in a humidified 7% CO_2 incubator at 37°C as described (Shanks et al., 1994). In brief, cells were grown in F12 medium (Coon's Modification; Sigma-Aldrich), pH 7.0, supplemented with 5% FBS, 10 μM hypoxanthine, 40 nM aminoterpin, and 1.6 μM thymidine. For injection and indirect immunofluorescence, cells were seeded onto glass coverslips at 1.3×10^4 cells/cm² and cultured for 8–12 d (Ihrke et al., 1993; Shanks et al., 1994).

Microinjection

Cells grown on coverslips were placed in prewarmed, Hepes-buffered (20 mM, pH 7.0), serum-free medium (HSFM) and were injected over a 10–15-min period using an Transjector 5246 and Micromanipulator 5171 with commercially purchased microneedles (Eppendorf) and then placed in complete medium at 37°C to recover. The injected antibodies and SH2-GST (2–4 mg/ml) were prepared in PBS, pH 7.4. Injected cells were detected by staining for the injected antibodies directly with Alexa 488–conjugated secondary antibodies (3 μg/ml), or for the fusion protein, by first applying anti-GST primary antibodies (affinity-purified, rabbit polyclonal antibody, 2.5 μg/ml) followed by detection with Alexa 488–conjugated antibodies (3 μg/ml).

Immunofluorescence microscopy

Injected cells were incubated for 4 h at 37°C before fixation. Treated cells were incubated at 37°C in HSFM in the absence or presence of 100 nM wortmannin or 50 μM leupeptin (see figure legends for details). Cells were rinsed briefly in PBS and placed on ice, fixed with chilled PBS containing 4% paraformaldehyde for 1 min, and permeabilized with ice-cold methanol for 10 min (Ihrke et al., 1993). Cells were further processed for indirect immunofluorescence according to previously published methods (Ihrke et al., 1993, 1998) with the following primary antibodies: anti–ASGP-R, –M6P-R, –MRP2, –LGP-120, –cathepsin D, -APN and -syntaxin13 (rabbit polyclonals, 1:100, 1:200, 1:200, 1:200, 1:200, 1:300, and 1:1,000, respectively), anti-5′NT, –endolyn-78, –EEA1, –DPP IV, and –GM10 (mouse monoclonal ascites, 1:500, 1:50, 1:100, and 1:100, respectively). Cells stained for rab5 (affinity-purified rabbit polyclonal antibody, 1:200) were prepermeabilized for 2 min at room temperature with PBS containing 0.2% Triton X-100. After rinsing with PBS, the cells were fixed with 4% paraformaldehyde/PBS for 30 min at room temperature. The secondary antibodies (Alexa 488– or 568–conjugated) were used at 3–5 μg/ml. For experiments using lysotracker, cells were treated with 100 nM wortmannin for 3 h at 37°C. During the last 30 min of incubation, 50 nM lysotracker (Molecular Probes) was added to the medium. After extensive rinsing with prewarmed medium, live cells were imaged directly by epifluorescence.

Preparation of samples for biochemical analysis

WIF-B cells were treated with 100 nM wortmannin in HSFM for the desired times at 37°C. The medium was aspirated and the cells detached by adding trypsin (137 mM NaCl, 5.4 mM KCl, 0.5 mM EDTA, 0.058% NaHCO₃, 0.05% trypsin, pH 7.4) and pelleted by centrifugation. The cells were resuspended in 5 ml of ice-cold swelling buffer (1 mM MgCl₂, 1 mM DTT, 1 mM EGTA) and incubated for 5 min on ice. Cells were pelleted by centrifugation, resuspended to a final concentration of $10–20 \times 10^6$ cells/ml in 0.25 M sucrose, 3 mM imidazole, pH 7.4, with added protease inhibitors (1 μg/ml each of leupeptin and antipain, 1 mM each of PMSF and benzamidine and 100 KIU/ml trasylol), and homogenized for 10 strokes with a loose fitting pestle in a Dounce homogenizer. The extracts were ei-

ther mixed with SDS-PAGE sample buffer directly or centrifuged for 45 min at 125,000 g at 4°C. The resultant pellet was resuspended to volume and both the supernatant and pellet samples were mixed with SDS-PAGE sample buffer and separated by gel electrophoresis. Polypeptides were transferred onto nitrocellulose and the Western blots were assayed for immunoreactivity with anti-EEA1 (rabbit polyclonal; 1:5,000) and ECL detection of HRP-conjugated secondary antibodies (Amersham Pharmacia Biotech). The relative levels of immunoreactive species were determined by densitometric comparison of immunoreactive bands (Microcomputer Imaging Device, Imaging Research, Inc.).

Trafficking assay

The transcytosis assays were performed as described (Ihrke et al., 1998). In brief, injected cells were recovered for 2 h at 37°C and then placed on ice for 5 min. Cells were labeled at 4°C for 15 min with anti-5′NT (IgG purified from monoclonal ascites using EZ-Sep (Amersham Pharmacia Biotech; 20 μg/ml) diluted in HSFM containing 2 mg/ml BSA. Since tight junctions restrict antibody access to the apical surface, only the 5′NT molecules present at the basolateral surface were labeled. The cells were washed in HSFM containing 2 mg/ml BSA then placed in complete medium, returned to 37°C, and incubated for 3 h. The cells were fixed and permeabilized as described above and the trafficked antibodies were labeled with Alexa 568–conjugated secondary antibodies (5 μg/ml). Injected cells were scored for the presence of intracellular 5′NT or for the relative immunofluorescence signal detected at the apical PM (see the legend to Fig. 4 for details). For experiments in Fig. 5, uninjected cells were labeled and antibodies were trafficked as above. After 5 h of chase at 37°C, cells were placed in HSFM and injected with anti-Vps34p. They were returned to complete medium, incubated an additional 4 h at 37°C, fixed, permeabilized, and labeled with secondary antibodies as described above. For experiments shown in Figs. 7 and 9, cells were pretreated for 2 h with 100 nM wortmannin. Antibodies diluted in HSFM containing 2 mg/ml BSA and 100 nM wortmannin were continuously applied for an additional hour at 37°C and the cells were processed as above. For Fig. 8, endolyn at the basolateral surface was continuously labeled for 1 h at 37°C and the cells processed as above.

Imaging

Immunofluorescence was analyzed using a laser scanning confocal microscope (Oz; Noran) for Figs. 1; 2; 3, a, b, e, and f; 5, a–f; and 8, a–d and m–f. For all other figures, labeled cells were visualized by epifluorescence (Axioplan Universal Microscope, ZEISS). Images were acquired with a Princeton MicroMax 1300Y cooled CCD camera (Roper Scientific) and IP Labs software (Scanalytics). Further image processing and figure compilation were done using Adobe Photoshop® and Microsoft PowerPoint software.

References

Backer, J.M. 2000. Phosphoinositide 3-kinases and the regulation of vesicular trafficking. *Mol. Cell. Biol. Res. Commun.* 3:193–204.

Barr, V.A., and A.L. Hubbard. 1993. Newly synthesized hepatocyte PM proteins are transported in transcytotic vesicles in the bile duct-ligated rat. *Gastroenterology.* 105:554–571.

Barr, V.A., L.J. Scott, and A.L. Hubbard. 1995. Immunoadsorption of hepatic vesicles carrying newly synthesized dipeptidyl peptidase IV and polymeric IgA receptor. *J. Biol. Chem.* 46:27834–27844.

Bomsel, M., K. Prydz, R.G. Parton, J. Gruenberg, and K. Simons. 1989. Endocytosis in filter-grown Madin-Darby Canine kidney cells. *J. Cell Biol.* 109:3243–3258.

Brown, W.J., D.B. DeWald, S.D. Emr, H. Plutner, and W.E. Balch. 1995. Role for phosphatidylinositol 3-kinase in the sorting and transport of newly synthesized lysosomal enzymes in mammalian cells. *J. Cell Biol.* 130:781–796.

Cardone, M., and K. Mostov. 1995. Wortmannin inhibits transcytosis of dimeric IgA by the polymeric immunoglobulin receptor. *FEBS Letts.* 376:74–76.

Corvera, S., and M.P. Czech. 1998. Direct targets of phosphoinositide 3-kinase products in membrane traffic and signal transduction. *Trends Cell Biol.* 8:442–446.

Dunn, W.A., T.P. Connolly, and A.L. Hubbard. 1986. Receptor-mediated endocytosis of epidermal growth factor by rat hepatocytes: receptor pathway. *J. Cell Biol.* 102:24–36.

Fruman, D.A., R.E. Meyers, and L.C. Cantley. 1998. Phosphoinositide kinases. *Annu. Rev. Biochem.* 67:481–507.

Fujita., M., F. Reinhart, and M. Neutra. 1990. Convergence of the apical and basolateral endocytic pathways at apical late endosomes in absorptive cells of suckling rat ileum in vivo. *J. Cell Sci.* 97:385–394.

Fujita, H., P.L. Tuma, C.M. Finnegan, L. Locco, and A.L. Hubbard. 1998. Endogenous syntaxins 2, 3, and 4 exhibit distinct but overlapping patterns of expression at the hepatocyte PM. *Biochem. J.* 329:527–538.

Gottlieb, T.A., I.E. Ivanov, M. Adesnik, and D.A. Sabatini. 1993. Actin microfilaments play a critical role in endocytosis at the apical but not the basolateral surface of polarized epithelial cells. *J. Cell Biol.* 120:695–710.

Hansen, S.H., A. Olsson, and J. Casanova. 1995. Wortmannin, an inhibitor of phosphoinositide 3-kinase, inhibits transcytosis in polarized epithelial cells. *J. Biol. Chem.* 270:28425–28432.

Herman, P.K., and S.D. Emr. 1990. Characterization of VPS34, a gene required for vacuolar protein sorting and vacuole segregation in *Saccharomyces cerevisiae. Mol. Cell. Biol.* 10:6742–6754.

Herman, P.K., J.H. Stack, J.A. DeModena, and S.D. Emr. 1991. A novel protein kinase homolog essential for protein sorting to the yeast lysosome-like vacuole. *Cell.* 64:425–437.

Hill, K., S. Welti, J. Yu, J.T. Murray, S.-C. Yip, J.S. Condeelis, J.E. Segall, and J.M. Backer. 2000. Specific requirement for the p85-p110α phosphatidylinositol 3-kinase during epidermal growth factor-stimulated actin nucleation in breast cancer cells. *J. Biol. Chem.* 275:3741–3744.

Holm, P.K., P. Eker, K. Sandvig, and B. van Deurs. 1995. Phorbol myristate acetate selectively stimulates apical endocytosis via protein kinase C in polarized MDCK cells. *Exp. Cell Res.* 217:157–168.

Ihrke, G., E.B. Neufeld, T. Meads, M.R. Shanks, D. Cassio, M. Laurent, T.A. Schroer, R.E. Pagano, and A.L. Hubbard. 1993. WIF-B cells: an in vitro model for studies of hepatocyte polarity. *J. Cell Biol.* 123:1761–1775.

Ihrke, I., G.V. Martin, M.R. Shanks, M. Schrader, T.A. Schroer, and A.L. Hubbard. 1998. Apical PM proteins and endolyn-78 travel through a subapical compartment in polarized WIF-B hepatocytes. *J. Cell Biol.* 141:115–133.

Jackman, M.R., W. Shurety, J.A. Ellis, and J.P. Luzio. 1994. Inhibition of apical but not basolateral endocytosis of ricin and folate in Caco-2 cells by cytochalasin D. *J. Cell Sci.* 107:2547–2556.

Jhun, B.H., D.W. Rose, B.L. Seely, L. Cantley, A.R. Saltiel, and J.M. Olefsky. 1994. Microinjection of the SH2 domain of the 85-kilodalton subunit of phosphatidylinositol 3-kinase inhibits insulin-induced DNA synthesis and c-fos expression. *Mol. Cell. Biol.* 14:7466–7475.

Keller, P., and K. Simons. 1997. Post-Golgi biosynthetic trafficking. *J. Cell Sci.* 110:3001–3009.

Kroschewski, R., A. Hall, and I. Mellman. 1999. Cdc42 controls secretory and endocytic transport to the basolateral plasma membrane of MDCK cells. *Nat. Cell Biol.* 1:8–13.

Leung, S.-M., W.G. Ruiz, and G. Apodaca. 2000. Sorting of membrane and fluid at the apical pole of polarized Madin Darby Canine Kidney cells. *Mol. Biol. Cell.* 11:2131–2150.

Llorente, A., O. Garred, P.K. Holm, P. Eker, J. Jacobsen, B. van Deurs, and K. Sandvig. 1996. Effect of calmodulin antagonists on endocytosis and intracellular transport of ricin in polarized MDCK cells. *Exp. Cell Res.* 227:298–308.

McBride, H.M., V. Rybin, C. Murphy, A. Giner, R. Teasdale, and M. Zerial. 1999. Oligomeric complexes link rab5 effectors with NSF and drive membrane fusion via interactions between EEA1 and syntaxin 13. *Cell.* 98:377–386.

Misra, S., P. Ujhazy, L. Varticovsky, and I.M. Arias. 1999. Phosphoinositide 3-kinase lipid products regulate ATP-dependent transport by sister of P-glycoprotein and multidrug resistance associated protein 2 in bile canicular membrane vesicles. *Proc. Natl. Acad. Sci. USA.* 96:5814–5819.

Panaretou, C., J. Domin, S. Cockcroft, and M.D. Waterfield. 1997. Characterization of p150, an adaptor protein for the human phosphatidyl inositol (PtdIns) 3-kinase. *J. Biol. Chem.* 272:2477–2485.

Parton, R.G., K. Prydz, M. Bomsel, K. Simons, and G. Griffiths. 1989. Meeting of the apical and basolateral endocytic pathways of the Madin-Darby Canine

Kidney cell in late endosomes. *J. Cell Biol.* 109:3259–3272.

Patki, V., J. Virbasius, W.S. Lane, B.-H. Toh, H.S. Shpetner, and S. Corvera. 1997. Identification of an early endosomal protein regulated by phosphatidylinositol 3-kinase. *Proc. Natl. Acad. Sci. USA.* 94:7326–7330.

Rahner, C., B. Stieger, and L. Landmann. 2000. Apical endocytosis in rat hepatocytes in situ involves clathrin, traverses a sub-apical compartment, and leads to lysosomes. *Gastroenterology.* 119:1692–1707.

Reaves, B.J., N.A. Bright, M. Mullock, and J.P. Luzio. 1996. The effect of wortmannin on the localisation of lysosomal type 1 integral membrane glycoproteins suggests a role for phosphoinositide 3-kinase activity in regulating membrane traffic late in the endocytic pathway. *J. Cell Sci.* 109:749–762.

Rordorf-Nikolic, T., D.J. Van Horn, D. Chen, M.F. White, and J.M. Backer. 1995. Regulation of phosphatidylinositol 3′-kinase by tyrosyl phosphoproteins. *J. Biol. Chem.* 270:3662–3666.

Shanks, M.S., D. Cassio, O. Lecoq, and A.L. Hubbard. 1994. An improved rat hepatoma hybrid cell line. Generation and comparison with its hepatoma relatives and hepatocytes in vivo. *J. Cell Sci.* 107:813–825.

Shepherd, P.R., B.J. Reaves, and H.W. Davidson. 1996. Phosphoinositide 3-kinases and membrane traffic. *Trends Cell Biol.* 6:92–97.

Shurety, W., N.A. Bright, and J.P. Luzio. 1996. The effects of cytochalasin D and phorbol myristate acetate on the apical endocytosis of ricin in polarised Caco-2 cells. *J. Cell Sci.* 109:2927–2935.

Siddhanta, U., J. McIlroy, A. Shah, Y. Zhang, and J.M. Backer. 1998. Distinct roles for p110α and hVPS34 phosphatidylinositol 3′-kinases in vesicular trafficking, regulation of the actin cytoskeleton, and mitogenesis. *J. Cell Biol.* 143:1647–1659.

Stenmark, H., and R. Aasland. 1999. FYVE-finger proteins-effectors of an inositol lipid. *J. Cell Sci.* 112:4175–4183.

Tuma, P.L., and A.L. Hubbard. 2001. The hepatocyte surface: dynamic polarity. *In* The Liver: Biology and Pathobiology. I.M. Arias et al., editors. Lippincott Williams and Wilkins, New York. 97–117.

Tuma, P.L., C.M. Finnegan, J.-H. Yi, and A.L. Hubbard. 1999. Evidence of apical endocytosis in polarized hepatic cells: phosphoinositide 3-kinase inhibitors lead to the lysosomal accumulation of resident apical plasma membrane proteins. *J. Cell Biol.* 145:1089–1102.

Van Dyke, R.W. 1996. Acidification of lysosomes and endosomes. *Subcell. Biochem.* 27:331–360.

Volinia, S., R. Dhand, B. Vanhaesebroeck, L.K. MacDougall, R. Stein, M.J. Zvelebil, J. Domin, C. Panaretou, and M.D. Waterfield. 1995. A human phosphatidylinositol 3-kinase complex related to yeast Vps34p-Vps15p protein sorting system. *EMBO J.* 14:3339–3348.

Wall, D.A., and A.L. Hubbard. 1985. Receptor-mediated endocytosis of asialoglycoproteins by rat liver hepatocytes: biochemical characterization of the endosomal compartments. *J. Cell Biol.* 101:2104–2112.

Wurmser, A.E., and S.D. Emr. 1998. Phosphoinositide signaling and turnover: PtdIns(3)P, a regulator of membrane traffic, is transported to the vacuole and degraded by a process that requires lumenal vacuolar hydrolase activities. *EMBO J.* 17:4930–4942.

Zheng, Y., S. Bagrodia, and R.A. Cerione. 1994. Activation of phosphoinositide 3-kinase activity by Cdc42Hs binding to p85. *J. Biol. Chem.* 269:18727–18730.